NANO LETTERS

xxxx
Vol. 0, No. 0
A−H

Nanoparticle Traffic on Helical Tracks: Thermophoretic Mass Transport through Carbon Nanotubes

Philipp A. E. Schoen,*,† Jens H. Walther,‡,§ Salvatore Arcidiacono,† Dimos Poulikakos,*,† and Petros Koumoutsakos‡

Laboratory of Thermodynamics in Emerging Technologies, ETH Zurich, CH-8092 Zurich, Switzerland, Institute of Computational Science, ETH Zurich, CH-8092 Zurich, Switzerland, and Department of Mechanical Engineering, Fluid Mechanics, Technical University of Denmark, DK-2800 Lyngby, Denmark

Received May 2, 2006; Revised Manuscript Received June 21, 2006

ABSTRACT

Using molecular dynamics simulations, we demonstrate and quantify thermophoretic motion of solid gold nanoparticles inside carbon nanotubes subject to wall temperature gradients ranging from 0.4 to 25 K/nm. For temperature gradients below 1 K/nm, we find that the particles move "on tracks" in a predictable fashion as they follow unique helical orbits depending on the geometry of the carbon nanotubes. These findings markedly advance our knowledge of mass transport mechanisms relevant to nanoscale applications.

Introduction. The ability of carbon nanotubes (CNT) to interact with materials at the molecular scale combined with their unique mechanical and electrical properties is leading to innovative nanoscale mass transport systems[1−4] such as nanoconveyors[5]. Simulations[1,3,6−9] and experiments[2,10] of mass flow inside CNTs demonstrated high transport rates when compared to equivalent pores and channels, respectively. However, no detailed study of the mass transport of solid nanoparticles inside CNTs is available at present. Because of the ability of CNTs to withstand high pressures, they can be used as robust nanoscale jigs for extruding and deforming hard nanomaterials and for modifying their properties.[11]

The use of CNTs for the controlled transport and deposition of solid material remains a subject of ongoing investigation because at present it still requires high temperatures and voltage. Identifying effective mechanisms and gaining fundamental understanding of mass transport inside CNTs is critical in order to realize technologies of this nature. The fabrication of nanoscale devices requiring transport of mass often follows the routes of chemical assembly including chemical deposition on patterned surfaces,[12] nanolithography,[13,14] and biological self-assembly.[12,15,16] For example, experimental investigations presented "nanocars" by verifying the temperature-driven rolling motion of wheel-like alkynyl-fullerenes[17] on a gold surface. Self assembly relies on gradients of the free energy to induce a controlled motion, positioning, and immobilization or fixation of the individual objects comprising the device. Free energy gradients used for self-assembly include hydrophobic interactions,[18] electrophoresis,[19] hydrogen bond formation,[20] and surface tension.[21−23]

Recent findings on the filling of CNTs with solid nanoparticles[3,24] provide a fertile ground for the generation of new ideas for controlled mass transport inside CNTs. As an example, recent simulations have demonstrated a biased, directional diffusion of copper nanoparticles confined inside CNTs at isothermal conditions.[25] In the present study, we analyze the directed thermal diffusion and movement on "tracks" of solid gold nanoparticles confined inside different CNTs subject to a thermal gradient.

Numerical Details. We performe both constrained and unconstrained molecular dynamics simulations using the molecular dynamics package FASTTUBE.[26] To this end, the CNT is modeled by a Morse bending, a harmonic cosine, and a torsion potential. With this model, we recover the experimental phonon frequencies in the graphene plane with an uncertainty less than 5%. The gold−gold interaction is modeled by the glue model.[27] The interaction between gold and carbon atoms is described by a 12−6 Lennard-Jones potential with $\epsilon_{Au,C} = 1.226$ kJ mol^{-1} and $\sigma_{Au,C} = 0.29943$

* Corresponding authors. E-mail: dimos.poulikakos@sl.ethz.ch; philipp.schoen@ethz.ch. Address: ETH Zurich, IET − LTNT, Sonneggstr. 3, CH-8092 Zurich, ML J 38. Fax: 0041/44 632 11 76. Phone: 0041/44 632 20 39 (D. Poulikakos).

† Laboratory of Thermodynamics in Emerging Technologies, ETH Zurich.

‡ Institute of Computational Science, ETH Zurich.

§ Department of Mechanical Engineering, Fluid Mechanics, Technical University of Denmark.

10.1021/nl060982r CCC: $33.50 © xxxx American Chemical Society
Published on Web 08/04/2006

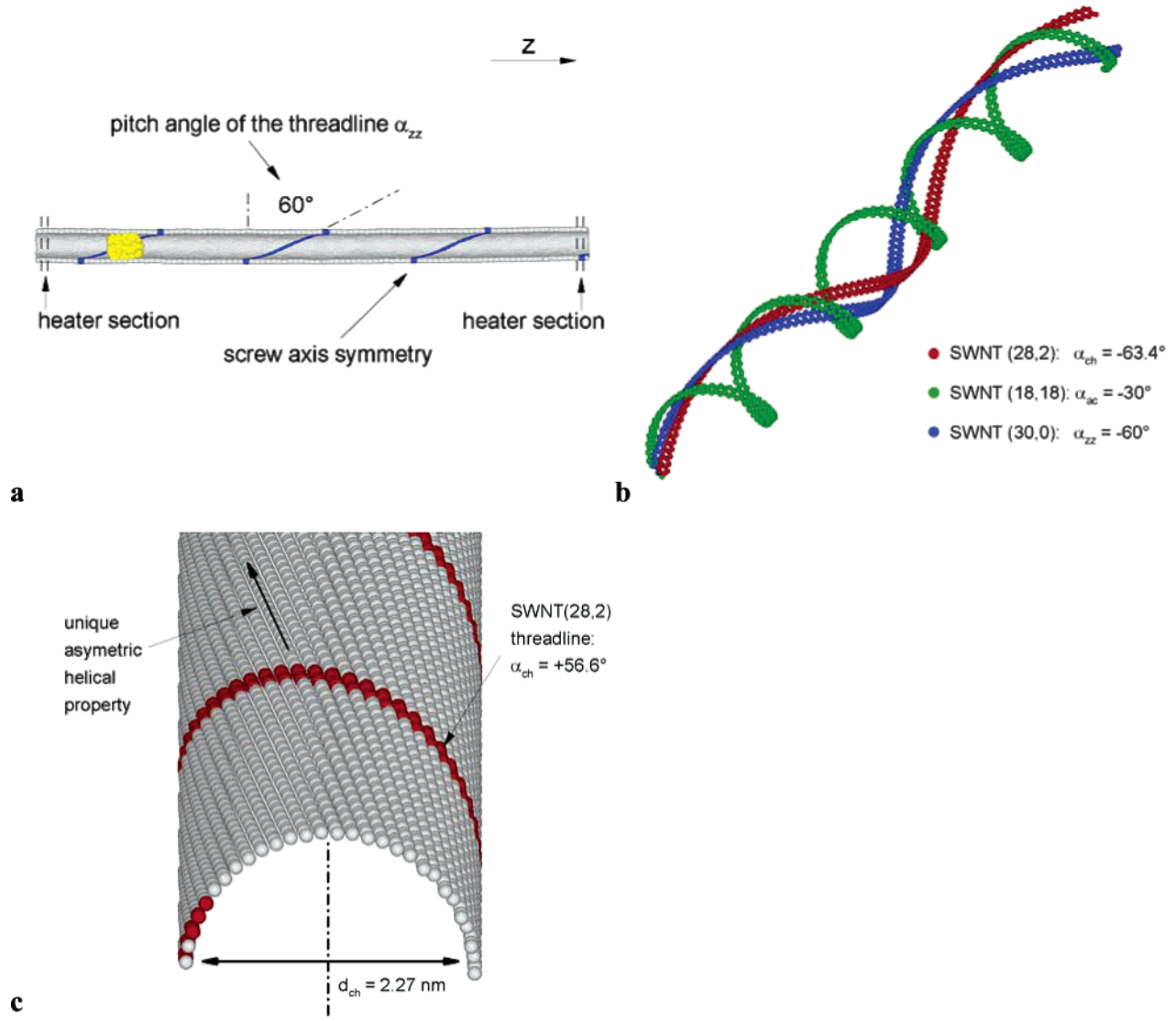

Figure 1. Computational domain and corrugation of carbon nanotubes. (a) Cross-sectional view of the 424 atoms gold nanoparticle (Au_{424}) confined inside a 21 nm long (30,0) zigzag CNT. The average diameter of the nanoparticle at 300 K is 1.72 nm. The cylindrical length of the particle is approximately 2 nm (likewise for Au_{775} in the armchair tube at 800 K: the diameter and length are 1.70 and 4.3 nm, respectively). A single atomic threadline of carbon atoms with a pitch angle of helical symmetry $\alpha_{zz} = 60°$ is shown in blue following the screw axis symmetry of a zigzag CNT. (b) One line of carbon hexagons containing two threadlines in the (28,2) chiral ($\alpha_{ch}^{-} \approx -63.4°$), (18,18) armchair ($\alpha_{ac} = -30°$), and (30,0) zigzag ($\alpha_{zz} = -60°$) CNT. Only the negative (clockwise) helical orientation is shown for clarity. (c) Cross-sectional view of the (28,2) chiral CNT showing the threadline in the positive direction ($\alpha_{ch}^{+} \approx +56.6°$) and the unique, asymmetric property of this chiral CNT in the same direction.

nm.[28] The constraint molecular dynamics simulations of this study employ the Berendsen thermostat[29] to impose a constant temperature in the range of 300−800 K. During the initial 2 ns equilibration, the system is weakly coupled to the thermostat with a coupling constant of 50 ps. The time step is set to 0.002 ps to resolve the lattice frequencies of the CNT adequately.

For the nonequilibrium molecular dynamics simulations, a temperature gradient is applied to the ends of the tube after equilibrium is reached. The CNT is fixed on both ends, with one end mounted on a heating source while the other is considered attached to a reservoir of high thermal inertia. We impose a constant temperature gradient by thermalizing only two 2 nm sections of the CNT (Figure 1a); that is, no thermostat is applied to the nonheated section between the ends of the CNT. A 0.5 nm section of the CNT is furthermore immobilized (zero net axial and rotational motion), mimicking a realistic situation of a nanotube bridging a gap between two points in a system.

All simulations performed here are summarized in Table 1, showing the constrained (setting the center of mass velocity, V_{CoM}) and unconstrained (temperature gradient) experiments.

Results. Here, we study the directed thermal diffusion of gold nanoparticles confined inside different CNTs subject to a thermal gradient using unconstrained nonequilibrium molecular dynamics simulations. Two different CNTs are considered here, a zigzag CNT with a chirality vector of $C_h = (30,0)$ (Figure 1a) and an armchair CNT with $C_h = (17,17)$.

Table 1. Numerical Experiments[a]

carbon nanotube			gold nanoparticle			constraint		
C_h	d_{CNT} (nm)	length (nm)	atoms	d_{Au} (nm)	length (nm)	shape	∇T (K/nm)	V_{CoM}
(17,17)	≈ 2.30	≈ 42	Au_{775}	≈ 1.70	≈ 4.3	cylindrical	2.4−24	0.015
(18,18)	≈ 2.44	≈ 42	Au_{424}	≈ 1.72	≈ 2.0	cylindrical	0.4−2.0	0.005−0.030
(28,2)	≈ 2.27	≈ 42	Au_{424}	≈ 1.72	≈ 2.0	cylindrical		0.010−0.030
(30,0)	≈ 2.35	≈ 42	Au_{424}	≈ 1.72	≈ 2.0	cylindrical	0.4−2.0	0.010−0.030
(30,0)	≈ 2.35	≈ 110	Au_{424}	≈ 1.72	≈ 2.0	cylindrical	0.4−0.6	
(50,0)	≈ 3.91	≈ 42	Au_{424}	≈ 2.00		spherical	0.4−2.0	

[a] Generally, the simulations can be divided in constrained (setting the center of mass velocity, V_{CoM}) and unconstrained (applying the temperature gradient, ∇T). Only for the calculation of the thermal force, both a temperature gradient and a constant center of mass velocity were applied as discussed in the text [Au_{775}−CNT(17,17)]. In the case of Au_{424}−CNT(18,18) and Au_{424}−CNT(30,0), either the temperature gradient was applied to test for the thermal force or the center of mass velocity was applied in order to calculated the helical atomic orbits.

The confined gold nanoparticles consist of 424 (Au_{424}) and 775 (Au_{775}) atoms so that these nanoparticles fill the entire cross section of the CNTs similar to those considerd in ref 30. The average diameter of the Au_{424} nanoparticle enclosed in the (30,0) zigzag CNT with CNT diameter of ∼2.35 nm is ∼1.72 nm at 300 K. The corresponding diameter (∼1.70 nm) for the Au_{775} nanoparticle enclosed in the (17,17) armchair CNT with CNT diameter of ∼2.30 nm is somewhat smaller because of the higher equilibrium temperature of 800 K. Thus, due to Pauli's principle, the van der Waals radii between the CNT walls and the gold nanoparticles are ∼0.315 nm at 300 K and 0.300 nm at 800 K, respectively. The cylindrical part of the larger Au_{775} nanoparticle is approximately twice as long as that of the Au_{424} particle (Figure 1a), see Table 1. The melting temperature of the Au_{424} and Au_{775} gold nanoparticles enclosed in these CNTs with tube diameters of approximately 2.30 nm is larger than 950 K.[30]

Temperature differences (ΔT) of 100, 200, 500, and 1000 K are imposed across the 42 nm of the armchair CNT (Au_{775}−CNT(17,17)), corresponding to temperature gradients (∇T) of approximately 2.4, 4.8, 12, and 24 K/nm. Likewise, temperature differences of 40 and 60 K are imposed across the longer zigzag CNT of 106 nm length (Au_{424}−CNT(30,0)) to test possible effects of the lengths of the CNT on the driving mechanism. This results in experimentally feasible temperature gradients of approximately 0.4 and 0.6 K/nm for the zigzag tube.

For all of the temperature gradients considered (0.4−24 K/nm), the nanoparticle experiences a directed motion in the direction opposite to the temperature gradient (Figure 2a), that is, from the hot to the cold region. For the high-temperature gradients (2.4−24 K/nm), a maximum terminal velocity is reached at 0.026, 0.042, 0.101, and 0.162 nm/ps (Au_{775}−CNT(17,17)). For the smaller temperature gradients (0.4−0.6 K/nm), the velocities range below 0.030 nm/ps (Au_{424}−CNT(30,0)). At the terminal velocity, the friction force acting between the two solid surfaces balances the driving thermal force. For the small temperature gradients, for example, 0.4 K/nm applied to the (30,0) zigzag CNT, the axial motion of the gold nanoparticle contains stop-and-go events (Figure 2b). Moreover, Figure 2c clearly indicates that the particle does not travel in a straight line through the tube but rotates around its longitudinal axis. Changes in the rotational direction (from clockwise to counterclockwise) can occur. This rotation during translation results in helical orbits of gold atoms and is correlated with the helical lattice symmetry of the CNT (Figure 1b). In the following section, the helical motion of the gold nanoparticle is discussed in the trajectory analysis while the driving force is discussed separately.

Trajectory Analysis. Carbon nanotubes are characterized by a specific symmetry given by their chirality vector C_h. Relative to the tube axis, "threadlines"[31] (S) of two aligned but shifted carbon atom chains are present in the circumferential, helical (Figure 1b and c), and tube axis directions depending on C_h. The corrugation of the carbon atom lattice of the CNT is smallest along the direction of these threadlines (Figure 1b). The angle between the tube axis and the hexagon helix is known as the chiral (pitch) angle α. The helical symmetry of CNT threadlines with pitch angle $\alpha = \tan^{-1}(z_0/r\ \Phi_0)$ resulting from the symmetry operator $[C_q^w|(na/q)]^t\ C_n^s\ U^n$ is

$$r_{tsu} = \left[r, (-1)^u\Phi_0 + 2\pi\left(\frac{wt}{q}\right), (-1)^u z_0 + \frac{tn}{q}a\right] \qquad (1)$$

by neglecting the n-fold rotation about the tube axis.[32] In this equation, a is the unit cell height, z_0 and Φ_0 are the polar coordinates of a certain carbon atom with r being the radius of the tube, $u = 0,1$, and $t = 0, \pm1, \pm2, ...$, and, for example, $q/n = 2$ and $w = 1$ for achiral tubes.[32] Threadlines in zigzag CNTs are arranged with pitch angles of $\alpha_{zz} = 0°$ (circumferential) and $\alpha_{zz} = \pm60°$ (helical, Figure 1b) relative to the tube axis direction, respectively, and have $\alpha_{ac} = \pm30°$ (helical, Figure 1b) and $\alpha_{ac} = 90°$ (tube axis) for all armchair tubes. Chiral tubes do not have the same symmetry as those in the case of armchair or zigzag CNTs; that is, the pitch angle of the threadline in the positive and negative direction, respectively, deviates. The chiral CNT presented in the following discussions (C_h = (28,2)) have pitch angles of helical symmetry relative to the tube axis of $\alpha_{ch}^{+} \approx +56.6°$ (Figure 1c), $\alpha_{ch} \approx \pm3.4°$, and $\alpha_{ch}^{-} \approx -63.4°$ (Figure 1b). Additional to the helical symmetry of the threadlines, an extra helical symmetry in the negative direction exists for this tube (Figure 1c).

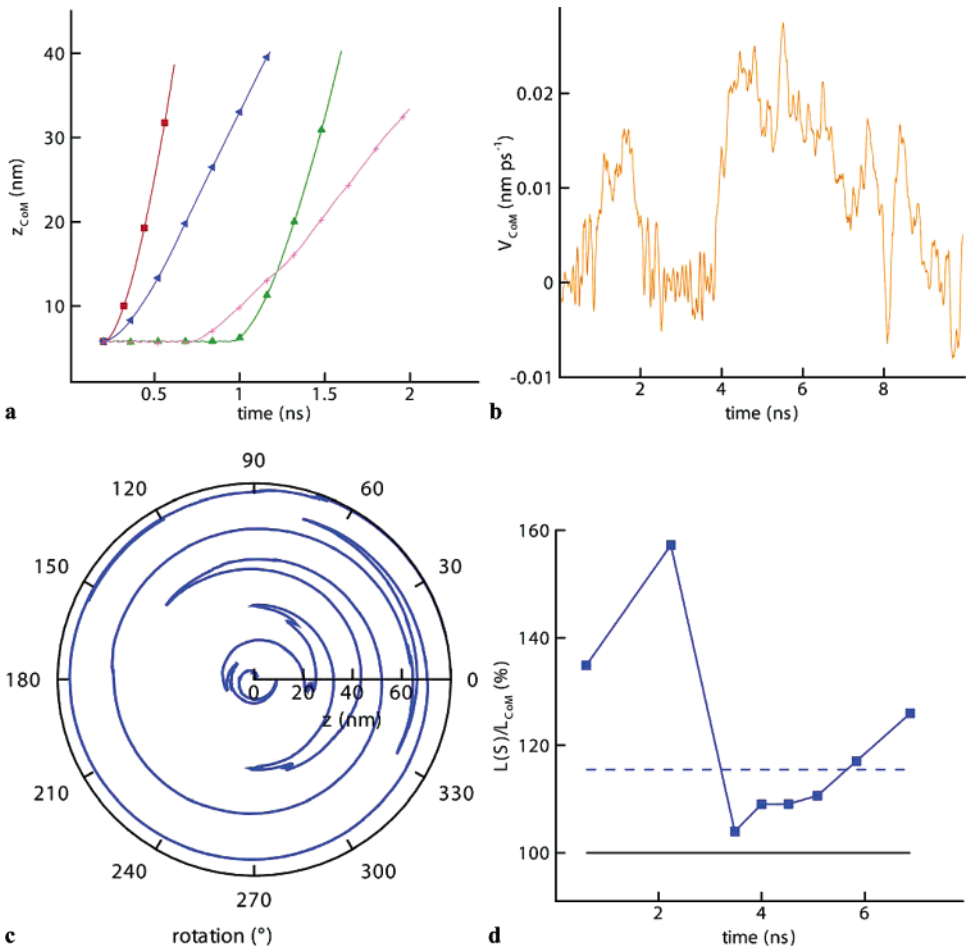

Figure 2. Unconstrained trajectories of the gold nanoparticle subject to a temperature gradient. (a) Time history of the center of mass (z_{CoM}) of an Au_{775} gold nanoparticle confined in a (17,17) armchair CNT. A temperature difference (ΔT) of 1000 K (solid squares, red), 500 K (solid delta, green), 200 K (solid triangle, blue), and 100 K (solid cross, purple) is imposed across the 42-nm-long CNT. (b) The time history of the center of mass velocity (V_{CoM}) of the Au_{424} nanoparticle confined inside a 106 nm (30,0) zigzag CNT subject to a temperature gradient of 0.4 K/nm at a mean temperature of 300 K. (c) Trajectory of a tracer atom located at the outermost gold shell as the nanoparticle travels through the tube subject to a temperature gradient of 0.4 K/nm. (d) The length of atomic trajectory $L(S_{Au})$ at different times relative to travel distance of the center of mass, L_{CoM} (solid squares, blue). The solid line represents pure translation, corresponding to L_{CoM}, and the dotted horizontal line represents the length of a helical line corresponding to the zigzag threadline with $\alpha_{zz} = 60°$, $L(S)$.

The helical symmetry of the CNT threadlines given by eq 1 can be approximated mathematically by a helical (screw) line $S(r,\phi,z) = [r\cos\phi, r\sin\phi, h\phi]$ and pitch angle $\alpha = \tan^{-1}(h/r)$. The length of this helical line is calculated by

$$L(S) = \int |S'(\phi)|\, d\phi \qquad (2)$$

with the prime denoting the derivative with respect to the angle ϕ. The angle in the $x-y$ plane is denoted by ϕ and h is the pitch of a spiral in the tube axis direction. For the particle trajectory, this equation is modified to approximate the helical, screw-like path of gold atoms orbiting around the center of mass of the nanoparticle while traveling through the CNT, that is, the change in local position with time as

$$L(S_{Au}) = \frac{1}{T}\left\langle \int_t \int_\phi \sqrt{\left(r_i^2 + \left(\frac{z_i}{|\phi_i|}\right)^2\right)} \cdot d\phi \cdot dt \right\rangle \qquad (3)$$

where r_i and z_i give the radius and axial position of gold atom i in the outermost shell at the gold−carbon interface. Note that the cylindrical part of the gold nanoparticle inside the CNT is structured in concentric shells around the tube axis.[30] The core radius r_i considers the offset of the gold from the carbon atoms due to Pauli's principle. The absolute value $|\phi_i|$ of the angle ϕ_i denotes the angle of a certain atom relative to the tube axis. Because of the symmetry of CNTs allowing the particle to do a clockwise and counterclockwise rotation along the threadlines of the tube, we considered the absolute value of the angle ϕ_i. The ensemble average is denoted by $\langle ... \rangle$. At temperatures considered in the constrained simulations, the nanoparticle is in the solid state; that is, the atom trajectories are highly correlated so that ensemble averaging is performed for 10 gold atoms contained in the outermost cylindrical shell of the gold nanoparticle. The integration considered all changes in ϕ_i of the particle trajectory traveling a certain distance along the tube axis, z. The second integration is performed over a period of time T for which the particle travels a distance of 20 nm (middle section of the tube to neglect boundary effects at the edges).

We correlate the helical (or screw-like) trajectory of the moving (simultaneous translation and rotation) nanoparticle with the CNT lattice symmetry. Thus, we compare the pitch angle (α_{tr}) and the length ($L(S_{Au})$) of the helical path (S_{Au}) of the gold atoms orbiting around the center of mass of the gold nanoparticle with corresponding values ($L(S)$ and α) of the helical, screw-like symmetry of the threadline (S) characterizing the CNT (Figure 1b). To this end, the path of single atoms in the outermost shell of the gold particle is traced and integrated over time (see eq 3). The length and pitch (chiral) angles of the helical threadline of the armchair ($L(S)_{30}$ and $\alpha_{ac} = \pm 30$) and zigzag ($L(S)_{60}$ and $\alpha_{zz} = \pm 60$) CNT are modeled by eq 2. All length scales are normalized by the distance traveled by the center of mass of the gold nanoparticle (L_{CoM}). Thus, a relative length ($L(S_{Au})/L_{CoM}$) larger than 100% indicates simultaneous rotation (orbiting) and translation and increases if the pitch angle of the helical line decreases.

For the small (0.4 K/nm) temperature gradient shown in Figure 2d, the relative length $L(S_{Au})/L_{CoM}$ ranges between 109% and 125% in the time span of approximately 4.2 ns and 7.5 ns (Figure 2d) corresponding to a center of mass velocity (V_{CoM}) of 0.020 nm/ps slightly decreasing to 0.010 nm/ps. During this time, the pitch angle of the atomic trajectory varies between $\alpha_{tr} \approx \pm 67°$ (at 4.2 ns, right after the acceleration) and $\alpha_{tr} \approx \pm 53°$ (at 7.5 ns). This is in reasonable agreement with the pitch angle of helical threadline for a zigzag CNT, $\alpha_{zz} = \pm 60°$ (Figure 1b). The corrugation of the CNT lattice is small along these threadlines so that the trajectory of the gold nanoparticle converges to these lines. During the stop-and-go phase at the beginning of the simulation (<4.2 ns, before acceleration) the relative length of the gold atoms trajectory in the outermost shell is increased (around 150%, Figure 2d), indicating oscillation of the particle around its longitudinal axis.

To study the helical motion of the gold nanoparticle in detail, we perform constrained molecular dynamics simulations at isothermal conditions (at 300 K). Thus, a constant velocity in the range of 0.005 nm/ps and 0.030 nm/ps is imposed to the center of mass of the particle equivalent to small temperature gradients between 0.4 and 1 K/nm. We study an armchair, a zigzag, and a chiral CNT with chiral vectors of C_h = (18,18), (28,2), and (30,0) corresponding to the diameters of approximately 2.44, 2.27, and 2.35 nm, and the length of the CNTs is 42 nm.

The results from the constraint molecular dynamics simulations shown in Figure 3a and b for the zigzag CNT (Au_{424}−CNT(30,0)) illustrate the helical orbit of a single gold atom similar to the unconstrained particle driven by a temperature gradient (shown in Figure 2c). The high-frequency oscillations at small velocities, for example, $V_{CoM} = 0.010$ nm/ps, observed in the trajectory is caused by diffusion around the rotational axis (Figure 3a). However, for a higher velocity $V_{CoM} = 0.015$ nm/ps and reduced oscillations (Figure 3b) the particle trajectory converges to the helical threadline of the zigzag CNT (pitch angle $\alpha_{zz} = \pm 60°$) as described by a measured pitch angle of the atomic trajectory of $\alpha_{tr} \approx \pm 60°$. At an axial position of approximately $z_{CoM} \approx 10$ nm and $z_{CoM} \approx 15$ nm, the particle rotation changes direction (Figure 3b).

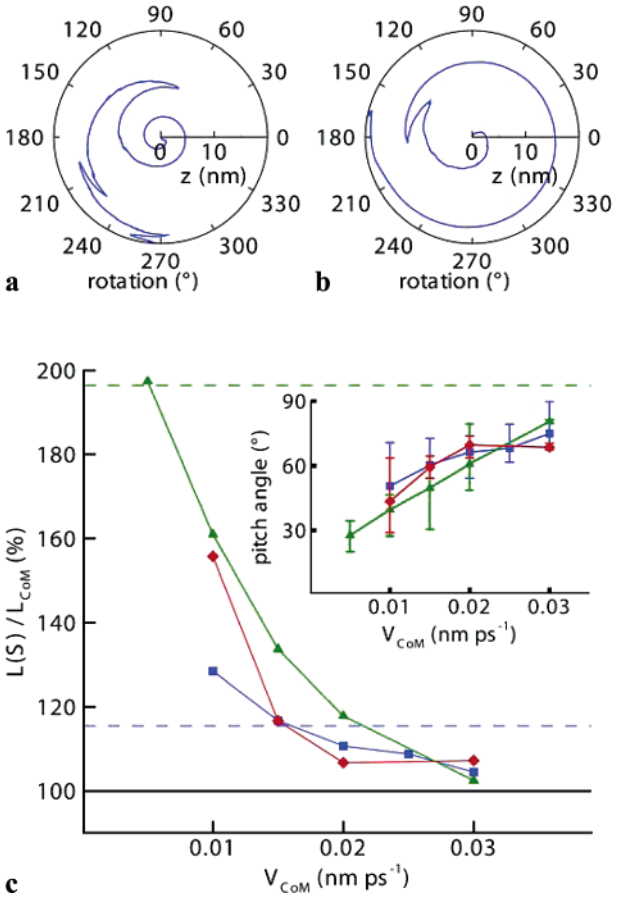

Figure 3. Constrained particle trajectories at steady-state, isothermal conditions. The trajectory of a gold tracer atom located in the outermost gold shell as the nanoparticle travels a distance of 20 nm through the tube. An Au_{424} nanoparticle subject to a constant velocity (V_{CoM}) inside a zigzag nanotube, Au_{424}−CNT(30,0), is shown for (a) $V_{CoM} = 0.010$ nm·ps^{-1} and (b) $V_{CoM} = 0.015$ nm·ps^{-1}. (c) The length of atomic trajectory $L(S_{Au})$ relative to the length of travel distance of the center of mass L_{CoM} is shown. The length of the helical line $L(S)$ of $\alpha_{zz} = \pm 60°$ (blue dashed horizontal line at $L(S)/L_{CoM} \approx 116\%$) and $\alpha_{ac} = \pm 30°$ (green dashed horizontal line at $L(S)/L_{CoM} \approx 196\%$) are included for comparison representing the helical threadline of zigzag and armchair CNTs, respectively. Symbols represent the arc length of the atomic trajectory $L(S_{Au})$ for the following configurations: Au_{424}−CNT(30,0) (filled squares, blue), Au_{424}−CNT(18,18) (solid delta, green), and Au_{424}−CNT(28,2) (solid diamonds, red) at a constant speed of center of mass (V_{CoM}) at an equilibrium temperature of 300 K. All length scales are normalized by the length of the trajectory of the center of mass L_{CoM}. Thus, a ($L(S_{Au})/L_{CoM}$) ratio of 100% indicates pure translation (without rotation) of the particle. The inset shows the pitch angle vs the velocity of center of mass, V_{CoM}. The uncertainty (represented by error bars) in the pitch angle is mainly caused by trajectory bifurcation, that is, the change in the rotational direction.

We observe no pure translation for the velocities considered (Figure 3c). The relative length of the helical atomic orbit ($L(S_{Au})/L_{CoM}$) for the Au_{424} gold nanoparticle inside the (30,0) zigzag CNT is about 105−130% depending on the speed of the particle with the smallest relative length corresponding to the highest velocity (V_{CoM}) of 0.030 nm/ps. The helical orbits have average pitch angles (α_{tr}) of approximately ±51°, ±60°, and ±66° at lower speeds (0.010,

0.015, and 0.020 nm/ps) and ±68° and ±75° at higher speeds (0.025 and 0.030 nm/ps) (inset of Figure 3c). This is in reasonable agreement with the helical threadline of a zigzag tube with $\alpha_{zz} = \pm 60°$ and in accordance with the results presented for the temperature-driven particle in the same tube.

In the case of the chiral (Au_{424}−CNT(28,2)) and armchair (Au_{424}−CNT(18,18)) carbon nanotubes, the relative length of the helical atomic orbit ($L(S_{Au})/L_{CoM}$) decreases quickly with increasing velocity corresponding to an increase of the measured pitch angle (α_{tr}). However, the relative length of the helical orbit ($L(S_{Au})/L_{CoM}$) inside the chiral CNT reaches a constant value for higher velocities $V_{CoM} \geq 0.020$ nm/ps at approximately 107% (Figure 3c) corresponding to a measured constant pitch angle of approximately 68°. Thus, no pure translation without simultaneous rotation exists even at a high speed of $V_{CoM} = 0.030$ nm/ps. Decreasing error bars of the pitch angle (less than 4%, inset of Figure 3c) indicate a unidirectional rotation that persists for an extended amount of time in the counterclockwise direction, which is explained by the unique, asymmetric helical property of the chiral tube in this direction (Figure 1c).

In the case of the armchair CNT, the relative length ($L(S_{Au})/L_{CoM}$) and pitch angle (α_{tr}) do not converge to constant values for higher velocities ($V_{CoM} \geq 0.020$ nm/ps). This is explained by the second threadline aligned with the tube axis ($\alpha_{tr} = 90°$) allowing the gold nanoparticle to travel on a straight trajectory without any rotation. The helical orbit is correlated to the CNT symmetry only for small velocities $V_{CoM} \leq 0.005$ nm/ps.

The uncertainty in pitch angles of the helical orbit for the armchair case is on the order of 15−27% compared to 8−15% for the zigzag case and 4−15% for the chiral case (inset of Figure 3c). The smaller values for the zigzag and chiral cases indicate that changes in rotational direction and superposed oscillation around the longitudinal axis at the threadline are less likely to occur and, in case of the chiral CNT, a unidirectional rotation persists. The higher probability of changing direction of rotation and oscillation, respectively, of the gold nanoparticle inside the armchair CNT may be explained by the difference in the surface corrugation when compared to the zigzag CNT. The resistance against relative rotation decreases with a decreasing standard deviation.[33] Therefore, we calculate the standard deviation of the cylindrical shape from a perfect cylinder from $\langle Dr_{c,i}(z)\rangle = \langle |r_{c,i}(z) - \langle r_{c,i}(z)\rangle|\rangle$,[34] thus quantifying the average deviation from a perfect circular shape at constant z along the tube axis. The deviation from perfect cylindrical shape for the whole armchair CNT is approximately 2.21%, whereas this deviation is slightly smaller for the zigzag CNT, 1.97%. For the cylindrical shell of the gold nanoparticle at the gold−carbon interface, the corresponding values are approximately 3.08% for gold enclosed in the armchair CNT (Au_{424}−CNT(18,18)) and 2.43% enclosed in the zigzag CNT (Au_{424}−CNT(30,0)). That is, in the case of Au_{424}−CNT(30,0) both the zigzag CNT and the gold nanoparticle are more cylindrical when compared to the system Au_{424}−CNT(18,18) of the armchair CNT. These values stay nearly constant up to temperatures of 800 K and increase slightly for higher temperatures. No helical motion is observed for $T > 1000$ K, which may be caused by the phase change of the gold nanoparticle.[30]

Force Analysis. To gain insight into the driving mechanism of the thermally induced solid transport, we performe another series of constrained but nonequilibrium molecular dynamics simulations in which we systematically vary the temperature gradient (∇T) and the mean temperature ($\bar{T}$). We note that for the present system the temperature gradient induces a difference in the capillary pressure (Δp) opposing the motion, as $\Delta p = -1/2\ R\Delta\gamma \cos\theta$, where R denotes the radius of the meniscus and $\Delta\gamma$ denotes the change in surface tension of the gold−carbon interface due to changes in the temperature, here $\Delta\gamma < 0$ for $\Delta T > 0$.[35] For the considered system, the contact angle θ exceeds 90°,[35] hence $\Delta p < 0$ for $\Delta T > 0$.

We study an Au_{775} particle confined inside a 42-nm-long (17,17) armchair CNT and extract from the simulation the force required to drive the particle through the CNT at a constant axial velocity. The imposed center of mass velocity is 0.015 nm/ps, sufficient low to ensure a velocity-independent force. The measured running average force $f(t)$ shown in Figure 4a is clearly harmonic, and we extract from this running average the mean thermal force $\bar{F}_{th}$ by fitting the data to the harmonic function

$$f(t) = A\cos\left(\frac{Ut}{\lambda} + \varphi\right) + \bar{F}_{th} \qquad (4)$$

where A, λ, and φ denote the amplitude, wavelength, and phase lag of the harmonic function. The extracted wavelength is 0.215 nm (Figure 4a) and is disparate from the peaks in the bulk radial distribution functions for gold−gold (0.286 nm), gold−carbon (0.2994 nm), and carbon−carbon (0.142, 0.246, and 0.284 nm). We perform phonon frequency calculations via the velocity autocorrelation function and find that the caps of the gold nanoparticle arrange themselves in an fcc-crystal structure, while the structure of the cylindrical part is helical. Specifically, at the grain boundary, in the vicinity of the moving contact line, the interatomic distance between the gold atoms is significantly smaller than that in bulk gold (Figure 4b and c). Thus, we expect that the harmonic oscillation in the thermal force is caused by such a pair of compressed gold atoms passing by a specific carbon atom of the nanotube. Even at this high temperature gradient, the average force (Figure 4a) displays instantaneous negative values, which at a low temperature gradient may result in a sticking behavior of the kind observed for the freely moving gold nanoparticles (Figure 2b).

To measure the force, we first vary the temperature gradient from 4.76 K/nm to 25 K/nm while keeping the mean temperature at 800 K. The resulting mean thermal force shown in Figure 4d is clearly linear, thus $F_{th} = K\nabla T$, with $K = 0.00345 \pm 0.00002$ kJ/mol·K. The linear proportionality is similar to that exhibited by a thermophoretic force in kinetic gas theory[36−38] but presents, to the authors' knowledge, the first observation of thermophoretic motion between two solids. Varying the mean temperature from 300 to 1000

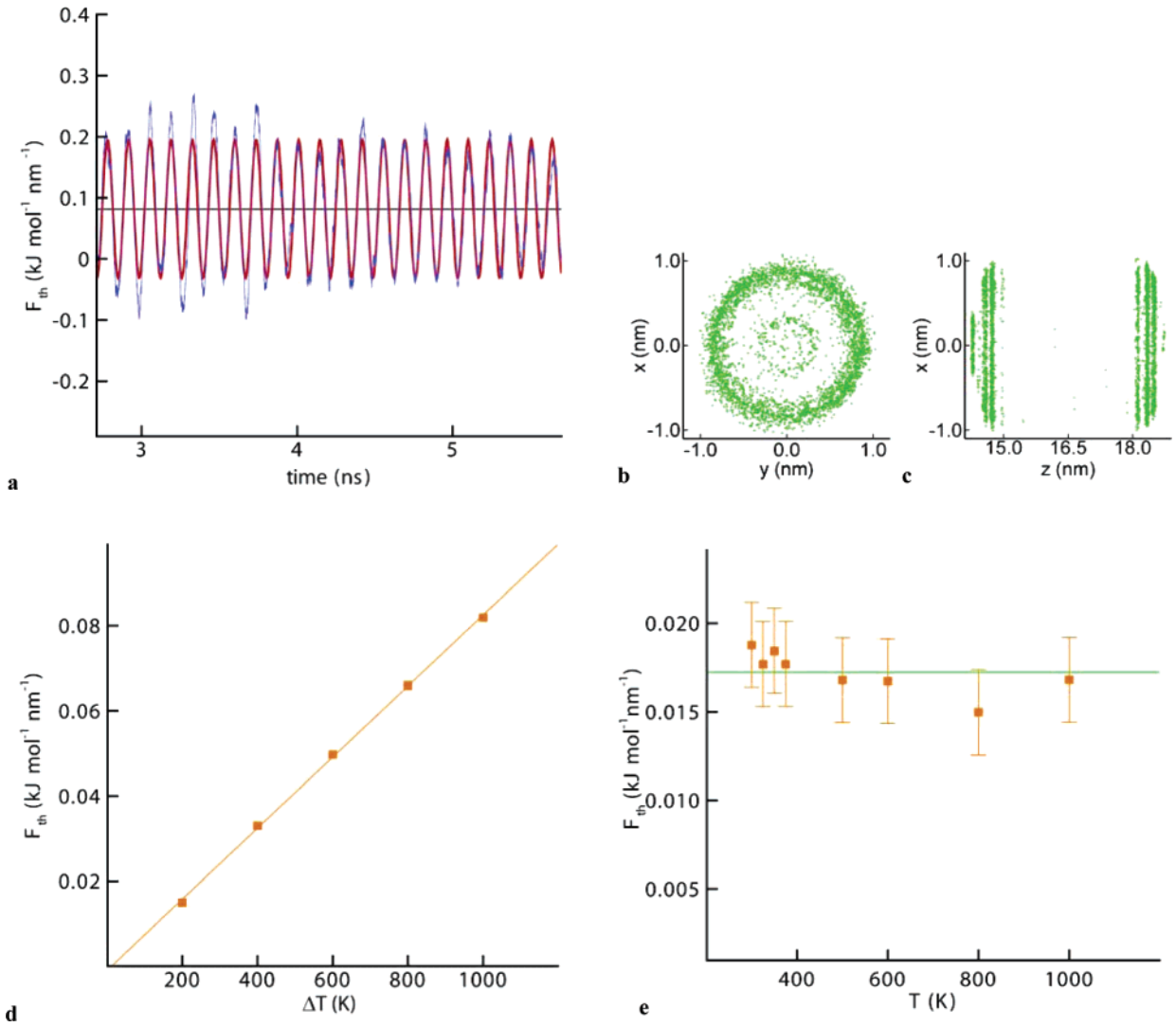

Figure 4. Force acting on the constrained gold nanoparticle moving in a carbon nanotube subject to a thermal gradient. (a) Time history of the total force acting on the moving Au_{775} gold nanoparticle in a (17,17) armchair CNT subject to a thermal gradient of 25 K/nm at a mean temperature of 800 K. The blue line shows the running time average force measured in the molecular dynamics simulation, and the red line represents the fitted harmonic function with an average value ($\bar{F}_{th}$) of 0.08145 kJ mol^{-1}nm^{-1}. (b and c) Pairs of gold atoms inside the Au_{775} nanoparticle located with an instantaneous distance less than 0.215 nm. (d) The thermal force acting on the Au_{775} gold nanoparticle subject to temperature gradients along the 42 nm long (17,17) armchair tube (solid triangles). The linear fit is given as a guide for the eyes. (e) Force on the Au_{775} particle subject to a temperature gradient of 4.76 K/nm at mean temperatures ranging from 200 to 1000 K.

K while keeping the thermal gradient constant at 4.76 K/nm, is observed to have a negligible influence on the thermal force (Figure 4e).

To exclude the possibility that the thermally driven motion of the nanoparticle is due to the conical shape of the CNT induced by the thermal contraction of the tube,[39−42] we study an additional configuration consisting of an Au_{424} particle inside a large 3.9-nm-diameter (50,0) zigzag CNT. The equilibrium structure consists of an approximately spherical gold nanoparticle with a diameter of 2 nm physisorbed to the inner wall of the CNT. This particle experiences a similar directed motion opposite of the temperature gradient (not shown here).

Conclusions. In summary, we have demonstrated that motion can be imparted on a solid gold nanoparticle confined inside a CNT subject to a temperature gradient. The study presents, to the best of our knowledge, the first observation of thermophoretic forces between two solid materials. Helical orbits of gold atoms inside the CNT are documented for temperature gradients not exceeding 1 K/nm, correlating with the lattice symmetry of the CNT. The results of the present simulations are intriguing because they demonstrate unique thermally driven mass transport capabilities of CNTs and the influence of different CNT symmetries on the trajectory (transport "on tracks") of solid gold nanoparticles.

Acknowledgment. This work was supported by the Swiss National Science Foundation under Grant No. 2000-067738/1.

References

(1) Hummer, G.; Rasaiah, J. C.; Noworyta, J. P. *Nature* **2001**, *414*, 188−190.
(2) Majumdar, M.; Chopra, N.; Andrews, R.; Hinds, B. J. *Nature* **2005**, *438*, 44.
(3) Supple, S.; Quirke, N. *Phys. Rev. Lett.* **2003**, *90*, 214501.

(4) Zimmerli, U.; Gonnet, P. G.; Walther, J. H.; Koumoutsakos, P. *Nano Lett.* **2005**, *5*, 1017−1022.
(5) Regan, B. C.; Aloni, S.; Ritchie, R. O.; Dahman, U.; Zettl, A. *Nature* **2004**, *428*, 924−927.
(6) Bhatia, S.; Chen, H.; Sholl, D. S. *Mol. Sim.* **2005**, *31*, 643.
(7) Chen, H.; Johnson, J. K.; Sholl, D. S. *J. Phys. Chem. B* **2006**, *110*, 1971.
(8) Skoulidas, A. I.; Sholl, D. S.; Johnson, J. K. *J. Chem. Phys.* **2006**, *124*, 054708.
(9) Skoulidas, A. I.; Ackerman, D. M.; Johnson, J. K.; Sholl, D. S. *Phys. Rev. Lett.* **2002**, *89*, 185901-1.
(10) Holt, J. K.; Park, H. G.; Wang, Y.; Stadermann, M.; Artyukhin, A. B.; Grigoropoulos, C.; Noy, A.; Bakajin, O. *Science* **2006**, *312*, 1034.
(11) Sun, L.; Banhart, F.; Krasheninnikov, A. V.; Rodriguez-Manzo, J. A.; Terrones, M.; Ajayan, P. M. *Science* **2006**, *312*, 1199.
(12) Wei, B. Q.; Vajtai, R.; Jung, Y.; Ward, J.; Zhang, R.; Ramananth, G.; Ajayan, P. M. *Nature* **2002**, *416*, 495.
(13) Piner, R. D.; Zhu, J.; Xu, F.; Hong, S. H.; Mirkin, C. A. *Science* **1999**, *283*, 661−663.
(14) Chung, S.-W.; Ginger, D. S.; Morales, M. W.; Zhang, Z.; Chandrasekhar, V.; Ratner, M. A.; Mirkin, C. A. *Small* **2005**, *1*, 64−69.
(15) Terfort, A.; Bowden, N.; Whiteside, G. M. *Nature* **1997**, *386*, 162−164.
(16) Vauthey, S.; Santoso, S.; Gong, H.; Watson, N.; Zhang, S. *Proc. Natl. Acad. Sci.* **2002**, *99*, 5355−5360.
(17) Shirai, Y.; Osgood, A. J.; Zhao, Y.; Kelly, K. F.; Tour, J. M. *Nano Lett.* **2005**, *5*, 2330.
(18) Choi, Y. S.; Yamamura, A.; Murakami, Y.; Yokoyama, K.; Kwon, Y. S.; Tamiya, E. *Mol. Cryst. Liq. Cryst.* **2001**, *371*, 407−410.
(19) Seo, H. W.; Han, C. S.; Choi, D. G.; Kim, K. S.; Lee, Y. H. *Microlelectron. Eng.* **2005**, *81*, 83−89.
(20) MacGillivary, L. R.; Atwood, J. L. *Nature* **1997**, *389*, 469−472.
(21) Lee, L.; Kim, C. J. *J. Microelectromech. Syst.* **2000**, *9*, 171−180.
(22) Gu, Z.; Chen, Y.; Gracias, D. H. *Langmuir* **2004**, *20*, 11308−11311.
(23) Raut, V. P.; Agashe, M. A.; Stuart, S. J.; Latour, R. A. *Langmuir* **2005**, *21*, 1629−1639.
(24) Ajayan, P. M.; Iijima, S. *Nature* **1993**, *361*, 333−334.
(25) Hwang, H. J.; Kwon, O.-K. K.; Kang, J. W. *Solid State Commun.* **2004**, *129*, 687−690.
(26) Walther, J. H.; Jaffe, R.; Halicioglu, T.; Koumoutsakos, P. *J. Phys. Chem. B* **2001**, *105*, 9980−9987.
(27) Ercolessi, F.; Parrinello, M.; Tosatti, E. *Philos. Mag. A* **1988**, *58*, 213−226.
(28) Luedtke, W. D.; Landman, U. *Phys. Rev. Lett.* **1999**, *82*, 3835−3838.
(29) Berendsen, H. J. C.; Postma, J. P. M.; van Gunsteren, W. F.; DiNola, A.; Haak, J. R. *J. Chem. Phys.* **1984**, *81*, 3684−3690.
(30) Arcidiacono, S.; Walther, J. H.; Poulikakos, D.; Passerone, D.; Koumoutsakos, P. *Phys. Rev. Lett.* **2005**, *94*, 105502.
(31) Belikov, A. V.; Lozovik, Y. E.; Nikolaev, A. G.; Popov, A. M. *Chem. Phys. Lett.* **2004**, *385*, 72−78.
(32) Reich, S.; Thomsen, C.; Maultzsch, J. *Carbon Nanotubes: Basic Concepts and Physical Properties*; Wiley-VCA: Berlin, 2004.
(33) Lozovik, Y. E.; Popov, A. M. *Chem. Phys. Lett.* **2000**, *328*, 355−362.
(34) Lozovik, Y. E.; Popov, A. M. *Phys. Solid State* **2002**, *44*, 186−194.
(35) Lee, J.; Nakamoto, M.; Tanaka, T. *J. Mater. Sci.* **2005**, *40*, 2167−2171.
(36) Brock, J. R. *J. Colloid Sci.* **1962**, *17*, 768.
(37) Maxwell, J. C. *Philos. Trans. R. Soc.* **1879**, *170*, 231−256.
(38) Talbot, L.; Cheng, R. K.; Schefer, R. W.; Willis, D. R. *J. Fluid. Mech.* **1980**, *101*, 737−758.
(39) Keblinski, P.; Schelling, P. K. *Phys. Rev. Lett.* **2005**, *94*, 209701.
(40) Kwon, Y.-K.; Berber, S.; Tomanek, D. *Phys. Rev. Lett.* **2004**, *92*, 015901−1.
(41) Schelling, P. K.; Keblinski, P. *Phys. Rev. B* **2003**, *68*, 035425.
(42) Yoshida, Y. *Rigaku J.* **2002**, *19*, 42−46.

NL060982R